Journal of Cluster Science (2022) 33:593–602
https://doi.org/10.1007/s10876-021-01991-z

ORIGINAL PAPER

# The Degradation Rate Study of Methyl Orange Using MWCNTs@$TiO_2$ as Photocatalyst, Application of Statistical Analysis Based on Fisher's F Distribution

Sedigheh Abbasi[1]

Received: 16 August 2020 / Accepted: 26 December 2020 / Published online: 27 January 2021


**Abstract**
In this study the synthesized photocatalysts such as $TiO_2$ nanoparticles and MWCNTs@$TiO_2$ are applied for elimination of methyl orange (MO). The results confirm that the MO concentration is reduced by enhancement of irradiation time and weight fraction of photocatalysts. However, the degradation rate of MO using MWCNTs@$TiO_2$ is higher than that of $TiO_2$ nanoparticles. Statistical analysis of the degradation rate reveals that the influence of irradiation time is more that weight fraction. Meanwhile, the results of ANOVA depict that both of irradiation time and weight fraction have a reasonable effect on the degradation rate of MO. The hypothesis test confirms that the variation of the MO concentration can be successfully predicted using statistical models that contain all of the significant main factors and their interactions.

**Keywords** $TiO_2$ nanoparticles · MWCNTs@$TiO_2$ · Degradation rate · Statistical model · Hypothesis · ANOVA

## Introduction

Discharge of effluent from industrial plants, including textile industry in rivers and water systems, can cause serious problems for aquatic organisms. The presence of dyes in the discharged effluent reduces the penetration of sunlight into the deep water and the amount of dissolved oxygen in the water [1–3]. A large share of the colored pollutants that is produced in the whole world is related to the dyeing industry. Therefore, reducing the amount of dye contaminants present in the wastewater of industries seems to be an important issue and has received much attention in the recent years. Several methods have been investigated so far to remove dye contaminants such as reverse osmosis, filtration and activated carbon [4–7]. Although t these methods initially reduce the amount of contaminants, they do not completely eliminate pollutants. These methods only transfer pollutants from the effluent to another phase and cause secondary pollution [8, 9]. Advanced oxidation method is one of the applied methods for decomposition of dye contaminants [10, 11]. The basis of this technique is based on the use of semiconductors with wide band gap energy. According to the reported literatures, the most commonly used semiconductors are ZnO, $TiO_2$, and $SnO_2$ [2, 12–14]. The efficiency of the advanced oxidation method is strongly dependent on the stability of the created electrons and holes ($e^-$–$h^+$) pairs. Therefore, as long as the $e^-$–$h^+$ pairs are separated and no recombination takes place, they can successfully participate in the decomposition reactions. Therefore, one of the effective strategies to increase the efficiency of photocatalytic activity is to reduce the amount of $e^-$–$h^+$ pairs recombination [15, 16]. For this purpose, it must trap the excited electrons that are separated from the valence layer and transferred to the conduction layer in order to avoid being able to return to the capacitance layer. Binding of semiconductor photocatalysts to the surface of materials with high aspect ratio can delay the recombination of electrons and holes, thus leading to increased photocatalytic activity [17, 18]. Carbon nanotubes (CNTs) have been considered as a suitable choice for application in photocatalytic activities due to their unique properties such as acceptable catalytic activity, electronic properties, mechanical strength and porosity [19, 20]. Single-walled carbon nanotubes

✉ Sedigheh Abbasi
s.abbasi@esfarayen.ac.ir; abasi_1362@yahoo.com

[1] Central Research Laboratory, Esfarayen University of Technology, Esfarayen, North khorasan, Iran

(SWCNTs) and multi-walled carbon nanotubes (MWCNTs) are two most common types of carbon nanotubes [21, 22]. Due to the high cost and low production of single-walled carbon nanotubes, the use of single-walled carbon nanotubes is much lower than that of multi-walled carbon nanotubes. Conjunction of semiconductors to multi-walled carbon nanotubes facilitates electron transfer from the semiconductor capacitance layer and increases the amount of photocatalytic activity [23, 24]. Among semiconductor photocatalysts, titanium dioxide ($TiO_2$) nanoparticles have received much attention due to their wide band gap, mineralization ability of all organic compounds, disinfection of pathogenic microorganisms present in contaminated water, and considerable photocatalytic activity [25, 26]. Therefore, coupling of $TiO_2$ nanoparticles with MWCNTs improves UV absorption and Postpones electron–hole recombination. Hens, it can lead to the enhancement of photocatalytic activity and degradation of organic pollutants. Although there have been numerous studies on the photocatalytic activity of $TiO_2$ nanoparticles and MWCNTs@ $TiO_2$, no statistical investigation of the photocatalytic activity and the importance of experimental factors on the rate of contaminant removal have been reported. Therefore, in this study, $TiO_2$ nanoparticles are synthesized on the surface of MWCNTs. The obtained samples are applied as photocatalyst for decomposition of methyl orange (MO) as an organic pollutant. The photocatalytic results are analyzed based on the analysis of variance (ANOVA). Then the importance of the different factors (such as UV irradiation time and weight fraction of photocatalysts) on the variation of MO concentration is studied. Finally, the adequacy of the proposed statistical models is investigated.

## Experimental

### Materials

The used materials for synthesis of $TiO_2$ nanoparticles and MWCNTs@$TiO_2$ as photocatalysts are Tetra chloride titanium ($TiCl_4$, 99%, Merck), MWCNTs (95.9% purity, diameter: ~ 40–60 nm, length: ~ 5-15 μm) and Nitric Acid ($HNO_3$, M = 63, 65%, Merck). Methyl orange (99.5%, Merck) is used as an organic pollutant for evaluation of the photocatalytic activity of the synthesized samples.

### Preparation of $TiO_2$ nanoparticles

The $TiO_2$ nanoparticles are synthesized via hydrolysis method. For this purpose, 0.8 ml of $TiCl_4$ is dispersed into 100 ml of distilled water and the solution is stirred at room temperature for about 5 h. Then, the temperature of the prepared white solution is increase to 65 °C and maintain at this temperature for 12 h. It leads to the precipitation of the white powder that has amorphous structure. The collected powder is washed several times with distilled water and dried at 90 °C. Finally, the dried powder is calcined at 350 °C for 3 h.

### Preparation of MWCNTs@$TiO_2$

In the preparation process of MWCNTs@$TiO_2$, MWCNTs are applied as support for synthesis of $TiO_2$ nanoparticles. As MWCNTs have hydrophobic nature, the synthesis of $TiO_2$ nanoparticles on the surface of them is not possible without functionalization step. Therefore, the synthesis of MWCNTs@$TiO_2$ includes two steps. The first step is functionalization of MWCNTs with oxygen containing groups that lead to the dispersibility improvement of MWCNTs in the organic solvents and reducing the hydrophobicity. Functionalization of MWCNTs is carried out based on the reported method in the previous researches [27, 28]. In a typical, 0.1 g of as purchased MWCNTs is dispersed in 50 ml of $HNO_3$ and stirred for 2 h. Then the mixture is transferred into the ultrasonic bath for 2 h at room temperature. Subsequently, the suspension is filtered, washed several times with distilled water and dried at 80 °C for 12 h. The second step is synthesis of $TiO_2$ nanoparticles on the surface of MWCNTs as template. In this step, 0.04 g of functionalized MWCNTs is dispersed in 100 ml of distilled water. The obtained mixture is sonicated about 30 min. After the preparation of uniform mixture, 0.4 ml of $TiCl_4$ is slowly added to the mixture. The prepared suspension is agitated at room temperature for 5 h. then. Then the temperature of suspension is increased to 65 °C for 12 h. Finally, the suspension is filtered, washed and calcined at 350 °C for 3 h.

### Degradation of MO Using Synthesized Photocatalysts

The degradation of MO is evaluated using $TiO_2$ nanoparticles and MWCNTs@ $TiO_2$ as photocatalysts. The degradation reactions are carried out in a batch photo reactor that is quipped by UV lamp (150 W). The presence of the light source in the photo reactor leads to the enhancement of temperature during the experiments. Therefore, a water circulation is added to the photo reactor that can reduce the temperature of suspension and fixed at 24 °C. The influence of UV irradiation time (from 5 to 35 min) and the weight fraction of the synthesized photo catalysts (0.1%wt, 0.2%wt and 0.3%wt) on the decomposition of MO are investigated. In each experiment, the desired amount of $TiO_2$ nanoparticles and MWCNTs@

$TiO_2$ is suspended in a MO aqueous solution (10 mg/L). The obtained suspension is transferred to the dark box and stirred for 60 min. It can leads to the adsorption–desorption equilibrium. The adsorption intensity of MO is recorded at 464 nm using a Lambda EZ 201spectrophotometer (Perkin Elmer Company). The recorded adsorption intensity is assigned as $A_0$. The adsorption intensity can be successfully referred to the initial concentration of MO in the suspension ($C_0$). Then, the MO suspension containing photocatalyst is irradiated using UV light source. After each interval (5 min), 3 ml of suspension is discharged and filtered several times to elimination of the suspended photocatalysts. The adsorption intensity that is recorded at any time of interval is subjected to $A_t$ (corresponds to the concentration of MO at any time of irradiation, $C_t$). The degradation of MO is estimated using $C_t/C_0$.

### Statistical Investigation

The variance among the obtained experimental data can be detected base on Fisher's F distribution [29]. There are two hypothesizes such as null and alternative in this test. The mentioned hypothesizes can be explained as below:

$\mathbf{H_0}$ $\mu_1 = \mu_2$ Null hypothesis

$\mathbf{H_1}$ $\mu_1 \neq \mu_2$ Alternative hypothesis

$\mu_1$ is the observed variance as a result of a studied factor at a specified level and $\mu_2$ is variance as a result of a same factor at the other level. If the reported critical F-value at each level of probability is lower than the factor's F-value, the null hypothesis can be successfully rejected. It means that the change of factor's levels can lead to the variation of response. One of the common statistical methods for determining the amount of variance between data is the analysis of variance (ANOVA) method. In this technique, P-value and F-value approaches can be applied for the rejection of null hypothesis. The F-value of each factor can be estimated using the Eq. 1:

$$\mathrm{F-value} = \frac{\mathrm{MSS_{factor}}}{\mathrm{MSS_{error}}} \quad (1)$$

In the above equation, $\mathrm{MSS_{factor}}$ and $\mathrm{MSS_{error}}$ are refered to the sum of square of factors and error, respectively. So that, if the F-value of each studied factor is larger than the critical F-value at level of probability, the null hypothesis can be rejected. Meanwhile, as can be mentioned the null hypothesis can be rejected based on the P-value approach. In fact, if the P-value of each factor is less than the significance level, the null hypothesis can be rejected [23, 30].

## Results and Discussion

### FTIR Investigation

Fourier transform infrared (FTIR) spectrums of raw and functionalized MWCNTs are presented in Figs. 1 and 2, respectively. Based on the results of Fig. 1, it can be observed that there are four main peaks. The peaks in the range of from 1139 $cm^{-1}$ to 1179 $cm^{-1}$ are attributed to the stretching vibration of C–C bonding which present in the structure of MWCNTs. The absorbance peaks around 1570 $cm^{-1}$ may be referred to the C=C stretching of MWCNTs [20, 22]. The observed peak at 2925 $cm^{-1}$ can be confirmed the presence of asymmetrical stretching of $CH_2$. Besides the mentioned peaks in the Fig. 1, there is a broad peak at 3448 $cm^{-1}$. This peak can be corresponded to the vibration of hydroxyl groups (O–H) that is ascribed to the oscillation of carboxyl groups (HO-C=O) on the surface of MWCNTs [31]. The presence of carboxylic groups on the surface of raw MWCNTs can be due to the purification process of MWCNTs [32]. According to the FTIR spectra of functionalized MWCNTs (Fig. 2), it can be seen that several main peaks containing oxygen groups are introduced on the surface of MWCNs. For example, the absorbance peaks at 1057 $cm^{-1}$, 1112 $cm^{-1}$, 1164 $cm^{-1}$ and 1384 $cm^{-1}$ are attributed to the stretching vibration of C–O groups. Meanwhile, two absorptions appeared at around 3421 $cm^{-1}$ and 1638 $cm^{-1}$ may be assigned to the stretching vibration of O–H groups [20]. The detectable transmission band at 3421 $cm^{-1}$ is assigned to the O–H vibration of carboxyl groups. In addition to the above-mentioned peaks, there is another main peak around 1722 $cm^{-1}$, which is attributed to the presence of carboxyl groups (HO-C=O). The attachment of carboxylic groups on the outer surface of MWCNTs confirms the oxidation of several carbon atoms using $NH_3$. All of these oxygen

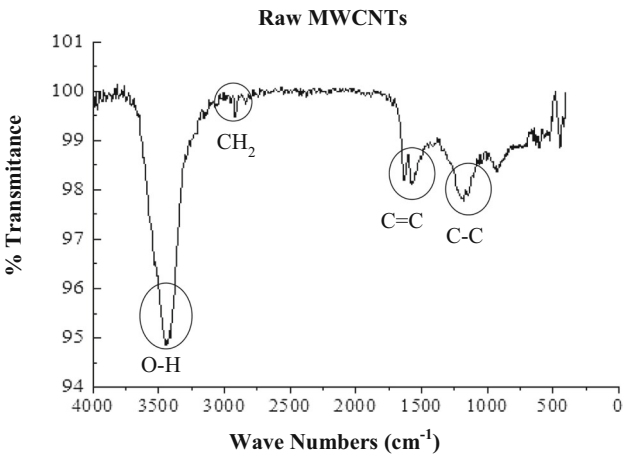


**Fig. 1** FTIR spectra of raw MWCNTs

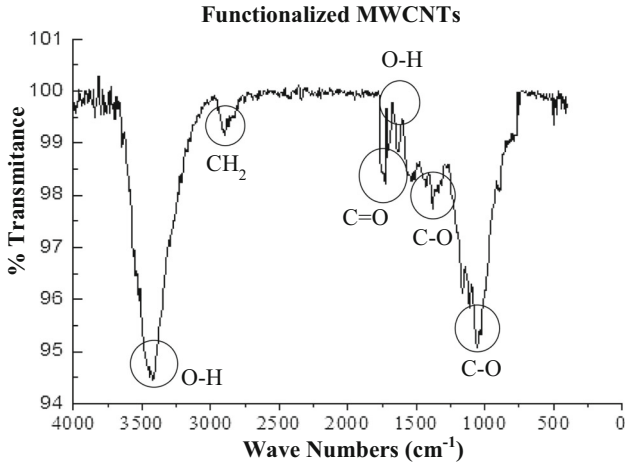


**Fig. 2** FTIR spectra of functionalized MWCNTs

containing groups are hydrophilic. Therefore, the presence of them on the surface of MWCNTs can eventuate the easily dispersion in the aqueous solutions.

Figure 3 presents the FTIR spectra of modified MWCNTs with $TiO_2$ nanoparticles. As can be seen, the transmission band around 1722 $cm^{-1}$ that is attributed to the stretching frequencies of C=O in the carboxylic groups ($–COO^-$) is disappeared. It can be due to the consumption of C=O groups during to the synthesis of $TiO_2$ nanoparticles on the sidewalls of MWCNTs [33]. In the other word, the attachment of the $TiO_2$ nanoparticles on the surface of MWCNTs is via to the covalent linkage. Therefore, the esterification process is carried out between C=O groups of MWCNTs and –OH groups of $TiO_2$ nanoparticles. Meanwhile, the introducing the $TiO_2$ nanoparticles on the sidewalls of MWCNTs leads to the decreasing the intensity of transmission bands around 3421 $cm^{-1}$ and 1638 $cm^{-1}$ that is corresponded to the O–H vibration of carboxylic groups. The other transmission band in the range of 430–550 $cm^{-1}$ is assigned to the vibration of Ti–O bond in the attached $TiO_2$ nanoparticles (O–Ti–O) on the surface of MWCNTs [33, 34]. Therefore, the presence of synthesized $TiO_2$ nanoparticles on the surface of MWCNTs can be confirmed.

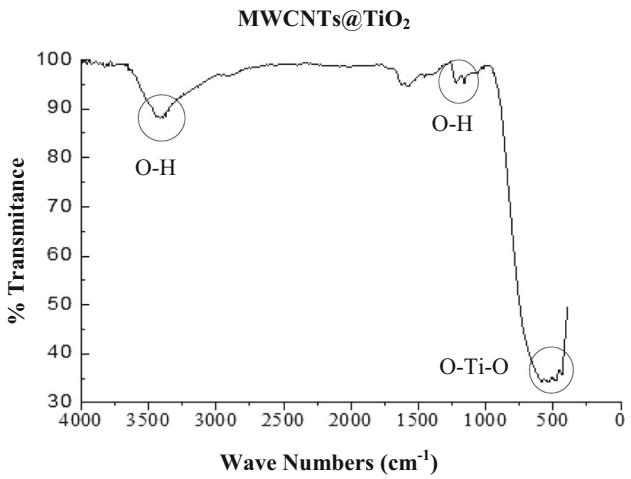


**Fig. 3** FTIR spectra of MWCNTs@$TiO_2$

## TEM Study

Figure 4 illustrates the TEM image of pristine MWCNTs. As can be seen, it is clear that the outer surface of MWCNTs is free of $TiO_2$ nanoparticles. Figure 5 shows the TEM image of the modified MWCNTs with $TiO_2$ nanoparticles. According to this Figure, it can be observed that $TiO_2$ nanoparticles are successfully introduced on the sidewalls of the functionalized MWCNTs. The produced oxygen containing groups (–COOH and –OH) on the sidewalls of MWCNTs during the acid treatment can act as active sites for the adsorption of soluble ions in the solution. Therefore, the generated $Ti^{+4}$ ions due to the hydrolysis of $TiCl_4$ can be adsorbed to the negative charges that are presented on the surface of MWCNTs [21, 22]. The electrostatic attraction between positive and negative ions leads to the nucleation of amorphous $TiO_2$ nanoparticles on the surface of MWCNTs. Finally, the calcination process eventuates to the synthesis of nanocrystals of $TiO_2$. According to the Fig. 6, it can be seen that the average particle size of the synthesized $TiO_2$ nanoparticles is in the range of from 6 to 14 nm. However, a larger percentage of the nanoparticles are 10 nm in size.

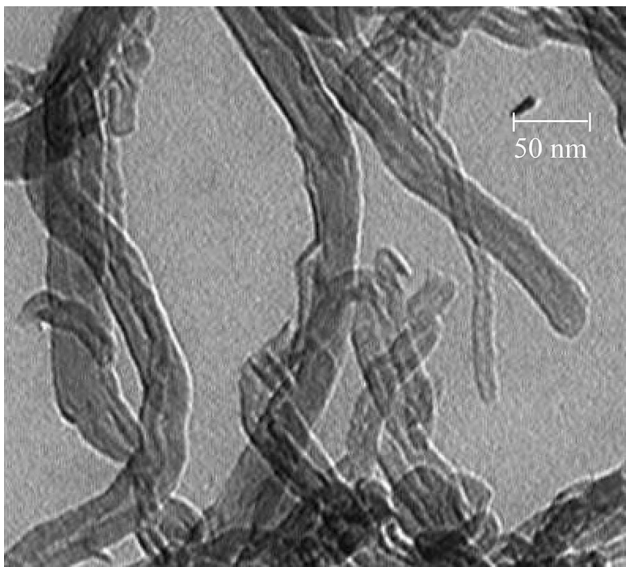


**Fig. 4** TEM image of pristine MWCNTs

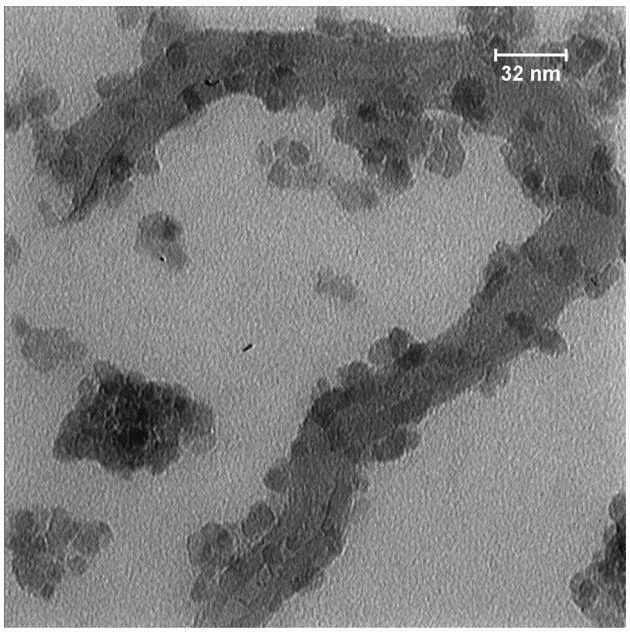


**Fig. 5** TEM image of modified MWCNTs with $TiO_2$ nanoparticles

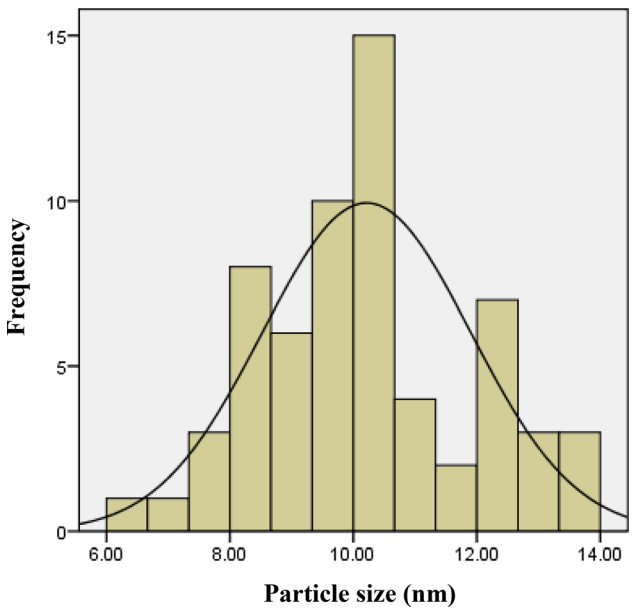


**Fig. 6** Particle size distribution of coated $TiO_2$ nanoparticles on the surface of MWCNTs

## Photocatalytic Activity Study

Figures 7 and 8 illustrate the photocatalytic degradation of MO using $TiO_2$ nanoparticles and MWCNTs@$TiO_2$, respectively. As can be seen, the ratio of final to initial concentration of MO decreases with respect to the irradiation time and weight fraction of applied photocatalysts. The decreasing of pollutant concentration with enhancement of irradiation time can be attributed to the effect of

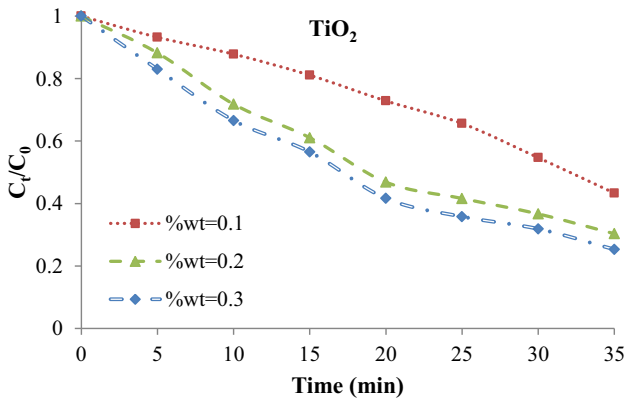


**Fig. 7** The influence of $TiO_2$ nanoparticles on the photocatalytic degradation of MO

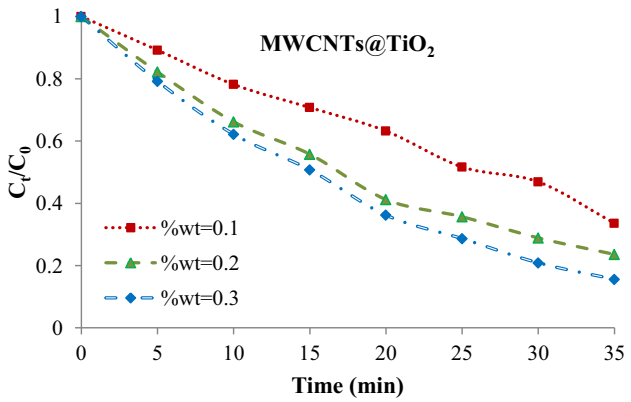


**Fig. 8** The influence of MWCNTs@$TiO_2$ on the photocatalytic degradation of MO

irradiation on the amount of produced electron–hole pairs ($e^-$–$h^+$). The degradation schematic of MO using using decorated MWCNTs with $TiO_2$ nanoparticles is illustrated in Fig. 9. Radiation of suspension containing pollutants and photocatalysts leads to the movement of electron from the valence band to the conduction band of photocatalysts. It can be eventuated to the generation of hole ($h^+$) and electron ($e^-$) at the valence band and conduction band, respectively. Hence, the transmitted electrons and generated $e^-$–$h^+$ pairs can be increased by enhancement of irradiation time. The produced $e^-$–$h^+$ pairs can be successfully converted to the active radicals such as $OH^{\cdot}$. The production mechanism of the oxidizing radicals is as Eqs. 2 to 7 [35]:

$$Semiconductor\ photocatalyst + h_v \rightarrow h^+ + e^- \quad (2)$$

$$e^- + O_2 \rightarrow \cdot O_2^- \quad (3)$$

$$\cdot O_2^- + 2H^+ + e^- \rightarrow H_2O_2 \quad (4)$$

$$H_2O_2 + e^- \rightarrow OH^{\cdot} + OH^- \quad (5)$$

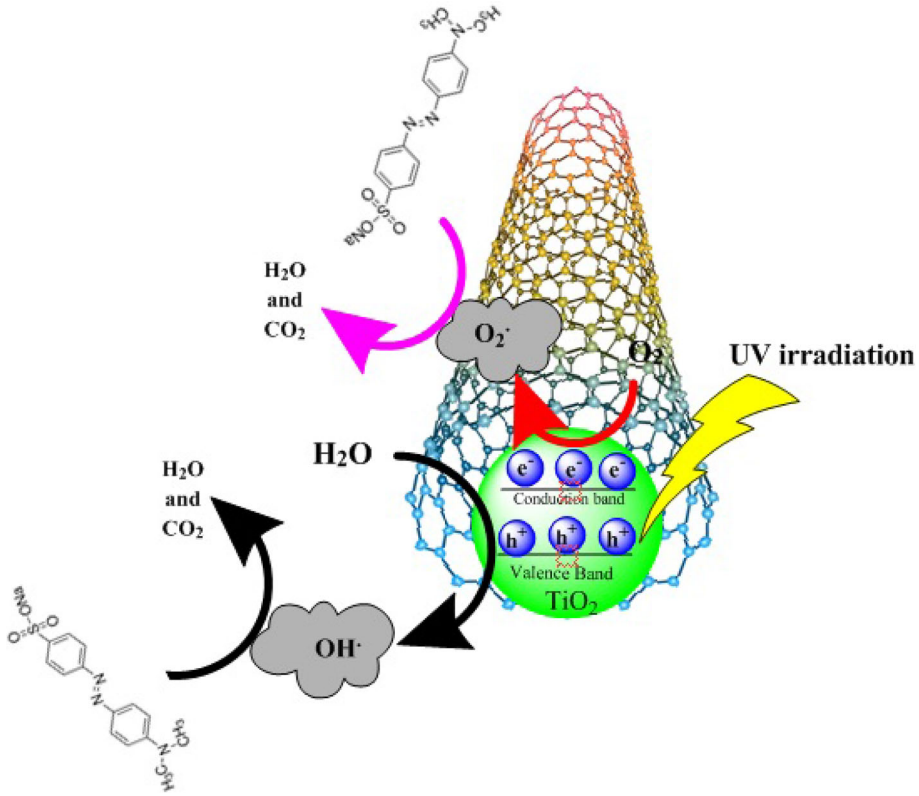


**Fig. 9** Degradation schematic of MO using decorated MWCNTs with $TiO_2$ nanoparticles

$$OH^- + h^+ \rightarrow OH^{\cdot} \quad (6)$$

$$OH^{\cdot} + MO\,molecules \rightarrow CO_2 + H_2O \quad (7)$$

The decreasing of MO concentration by enhancement of photocatalysts weight fraction can be attributed to the amount of transmitted electrons and active surface area. The enhancement of $TiO_2$ nanoparticles and MWCNTs@$TiO_2$ weight fractions leads to the augmentation of contact surface of photocatalysts and UV irradiation. Therefore, the amount of excited electrons can be enhanced. Thus, it can be confirmed that the production of active oxidant radicals such as $OH^{\cdot}$ increases [12, 36].

Figure 10 presents the comparison between photocatalytic degradation of MO using $TiO_2$ nanoparticles and MWCNTs@$TiO_2$. As can be seen, at three studied weight fractions of photocatalysts, the decomposition rate of MO using MWCNTs@$TiO_2$ is higher than that of $TiO_2$ nanoparticles. It may be due to the lower recombination rate of produced $e^-$–$h^+$ pairs in the synthesized MWCNTs@$TiO_2$ rather than $TiO_2$ nanoparticles. The main restriction in the decomposition of organic pollutants using semiconductor photocatalysts is the low efficiency due to the fast recombination of generated $e^-$–$h^+$ pairs. The recombination of $e^-$–$h^+$ pairs leads to the heat production without any decomposition reaction [15, 37]. Therefore, the degradation rate of semiconductor photocatalysts can be enhanced by decreasing the recombination rate of generated $e^-$–$h^+$ pairs. The decoration of semiconductor photocatalysts on the surface of materials with high aspect ratio such as MWCNTs can decrease the recombination rate of generated $e^-$–$h^+$ pairs. Therefore, the most of produced electrons can participate in the radicals production reactions. So, the amount of formed oxidant radicals in the synthesized MWCNTs@$TiO_2$ is higher than that of $TiO_2$ nanoparticles. Meanwhile, the agglomeration of $TiO_2$ nanoparticles as semiconductor photocatalyst can be decrease by decoration on the surface of MWCNTs [38]. Therefore, the active surface area of MWCNTs@$TiO_2$ is higher than that of $TiO_2$ nanoparticles. Thus, the amount of attached MO molecules on the surface of MWCNTs@$TiO_2$ is higher than that of $TiO_2$ nanoparticles. It can be eventuated to the enhancement of the decomposition of MO using MWCNTs@$TiO_2$ rather than $TiO_2$ nanoparticles.

## Statistical Analysis Study of Response

The ANOVA tables for variation of MO concentration using $TiO_2$ nanoparticles and MWCNTs@$TiO_2$ as applied photocatalysts are presented in Tables 1 and 2, respectively. As can be seen, both of main factors (irradiation time and weight fraction of photocatalysts) have a considerable influence on the concentration of MO at significance level equal to 5%. It means that the enhancement of irradiation time from 5 to 35 min and increasing the weight

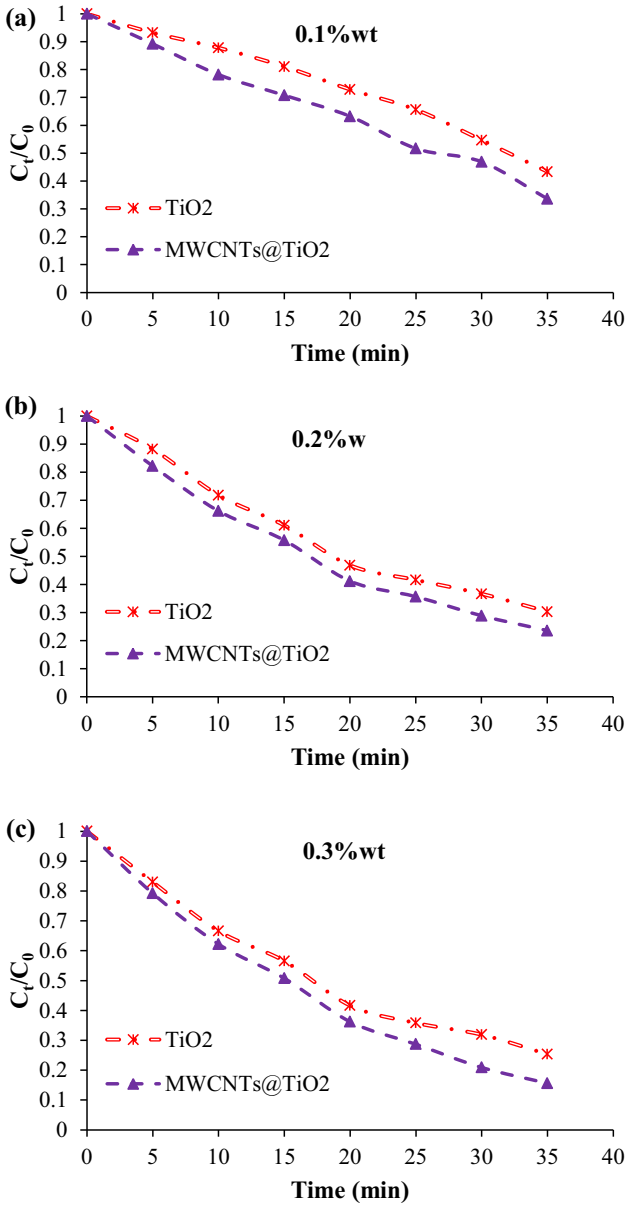


**Fig. 10** Comparison between influence of $TiO_2$ nanoparticles and MWCNTs@$TiO_2$ on the photocatalytic degradation of MO at different weight fraction, **a** 0.1%wt, **b** 0.2%wt, **c** 0.3%wt

fraction of $TiO_2$ nanoparticles and MWCNTs@$TiO_2$ up to 0.3%wt lead to the remarkable decreasing of MO concentration. The results of the analysis of variance also show that in addition to the main factors, the interaction between them (time-weight fraction, A-B) has P-value less than 0.05. Therefore, it can be concluded that the level variation of A-B can be significantly changes the MO concentration using both of $TiO_2$ nanoparticles and MWCNTs@$TiO_2$. Based on the Fisher's F-test, the F-value of each parameter indicates the importance of that factor. Thus, as the amount of F-value increases, the importance and effect of that factor on the response increases. Examination of the presented F-values related to irradiation time, weight fraction and their interaction shows that irradiation time has the most influence on the response and the order of their importance is A > B > A-B. The contribution percentage of irradiation time, weight fraction and their interaction on the removal of MO using $TiO_2$ nanoparticles is equal to 75.15%, 21.44% and 2.22%, respectively. Meanwhile, the contribution percentage of irradiation time, weight fraction and their interaction on the removal of MO using MWCNTs@$TiO_2$ is equal to 83.18%, 15.39% and 1.35%, respectively. Since all the main factors and their interactions are effective, the degree of freedom of lack of fit is zero. Therefore, it can be safely stated that the statistical models with the estimated coefficients that is presented in the Table 3 only include the effective factors. The correlation coefficient ($R^2$), F value, P-value and lack of fit are statistical parameters to check the accuracy of the presented models [39]. The lack of fit for the both of models is insignificant and the P-values of both of them are less than 0.05. As can be seen in Table 3, the $R^2$ values of proposed models using $TiO_2$ nanoparticles and MWCNTs@$TiO_2$ are equal to 0.9981 and 0.9991, respectively. Hence, all of the mentioned statistical parameters confirm that both of models have acceptable adequacy and accuracy for predicting changes in pollutant concentration.

Although all the mentioned statistical parameters confirm the validity of the proposed models for predicting the

**Table 1** ANOVA table for variation of MO concentration using $TiO_2$ nanoparticles as photocatalyst

| Source | Sum of square | Df | Mean Squares | F-Value | P-value | % Contribution | |
|---|---|---|---|---|---|---|---|
| Model | 2.73 | 20 | 0.14 | 1096.80 | < 0.0001 | – | Significant |
| A (Time) | 2.08 | 6 | 0.35 | 2789.52 | < 0.0001 | 75.15 | Significant |
| B (Weight Fraction) | 0.59 | 2 | 0.29 | 2355.63 | < 0.0001 | 21.44 | Significant |
| AB | 0.061 | 12 | 5.061E−03 | 40.64 | < 0.0001 | 2.22 | Significant |
| Lack of fit | 0 | 0 | – | – | – | 0.000 | Not significant |
| Pure error | 5.23E-03 | 42 | 1.245E−04 | – | – | 0.19 | – |
| Total | 2.74 | 62 | – | – | – | – | – |

**Table 2** ANOVA table for variation of MO concentration using MWCNTs@$TiO_2$ as photocatalyst

| Source | Sum of Square | Df | Mean Squares | F-Value | P-value | % Contribution | |
|---|---|---|---|---|---|---|---|
| Model | 2.89 | 20 | 0.14 | 2314.66 | < 0.0001 | – | Significant |
| A (Time) | 2.41 | 6 | 0.40 | 6423.24 | < 0.0001 | 83.18 | Significant |
| B (Weight Fraction) | 0.45 | 2 | 0.22 | 3564.36 | < 0.0001 | 15.39 | Significant |
| AB | 0.039 | 12 | 3.257E−03 | 52.09 | < 0.0001 | 1.35 | Significant |
| Lack of fit | 0 | 0 | – | – | – | 0.000 | Not significant |
| Pure error | 2.62E−03 | 42 | 6.252E−04 | – | – | 0.091 | – |
| Total | 2.90 | 62 | – | – | – | – | – |

**Table 3** The estimated coefficients for ratio of final to initial concentration of MO using applied photocatalysts in the proposed models

| Term | Estimated coefficients | |
|---|---|---|
| | $TiO_2$ nanoparticles | MWCNTs@$TiO_2$ |
| Intercept | 0.58 | 0.51 |
| A | 0.3 | 0.33 |
| $A^2$ | 0.18 | 0.18 |
| $A^3$ | 0.083 | 0.086 |
| $A^4$ | − 0.042 | − 0.036 |
| $A^5$ | − 0.10 | − 0.12 |
| $A^6$ | − 0.17 | − 0.18 |
| B | 0.13 | 0.11 |
| $B^2$ | − 0.041 | − 0.029 |
| AB | − 0.083 | − 0.058 |
| $A^2B$ | 9.958E−3 | − 0.021 |
| $A^3B$ | 0.015 | 2.381E−03 |
| $A^4B$ | 0.057 | 0.049 |
| $A^5B$ | 0.046 | 0.016 |
| $A^6B$ | 2.762E−03 | 0.032 |
| $AB^2$ | 0.042 | 0.015 |
| $A^2B^2$ | 5.048E−03 | 1.905E−03 |
| $A^3B^2$ | − 0.010 | − 4.762E−03 |
| $A^4B^2$ | − 0.028 | − 0.028 |
| $A^5B^2$ | − 0.020 | 1.429E-03 |
| $A^6B^2$ | − 2.952E−03 | − 4.762E−03 |
| $R^2$% | 0.9981 | 0.9991 |

response variations, the considered assumptions for the statistical analysis must also be investigated. The graphical analysis of the residuals is used to confirm the validity of the $TiO_2$ nanoparticles and MWCNTs@$TiO_2$ models and assumptions considered. Graphical statistical techniques explicitly show the relationship between the response and the studied parameters. One of the practical methods to prove the constant variance for the level of the studied factors and the independence of the error is to plot the curves of the residuals with respect to different independent variables, run number and the predicted values [40, 41]. Figures 11 and 12 show the sudentized residual versus predicted values for variation of MO concentration using $TiO_2$ nanoparticles and MWCNTs@$TiO_2$ nanoparticles, respectively. Given these Figures, it is observed that there is no specific pattern and relationship between the residuals changes with the predicted values by the models. Therefore, the normal distribution of residuals can be verified using these two Figures. In addition, the results show that all the studentized residuals are in the range of − 3 to 3 and there is no data out of range.

The outlier t plot of residuals for variation of MO concentration using $TiO_2$ nanoparticles and MWCNTs@$TiO_2$ are presented in Figs. 13 and 14, respectively. Evaluation of the experimental data using outlier test can be used to determine the improper deviation of residuals from the calculated responses. According to the Figs. 13 and 14, it

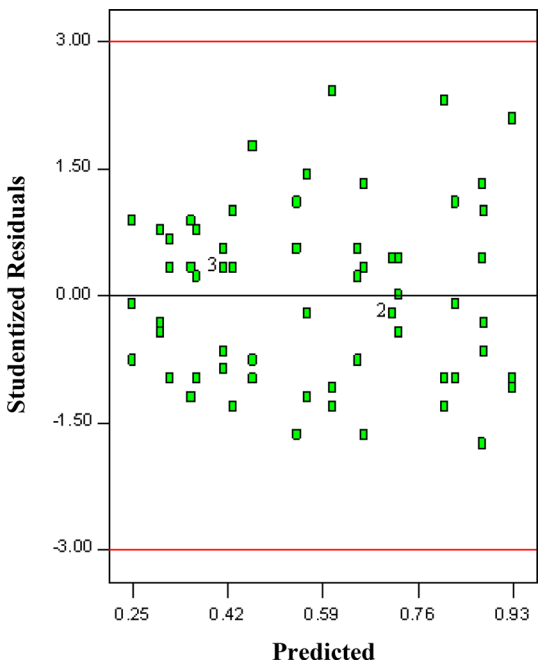


**Fig. 11** Studentized residual versus predicted plot for variation of MO concentration using $TiO_2$ nanoparticles

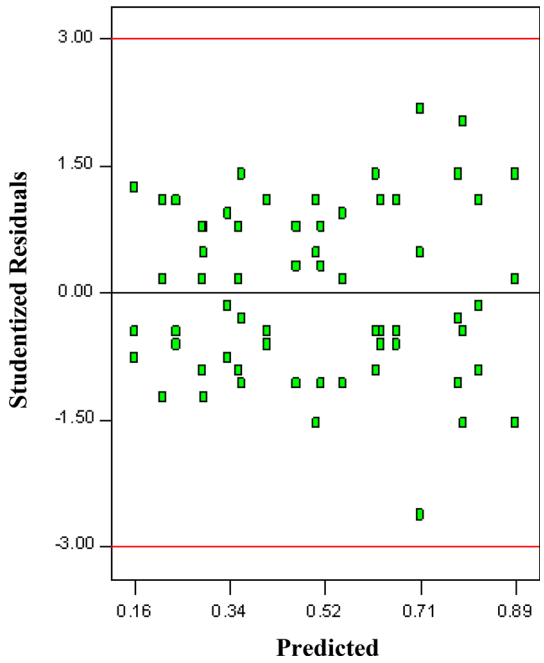


**Fig. 12** Studentized residual versus predicted plot for variation of MO concentration using MWCNTs@$TiO_2$

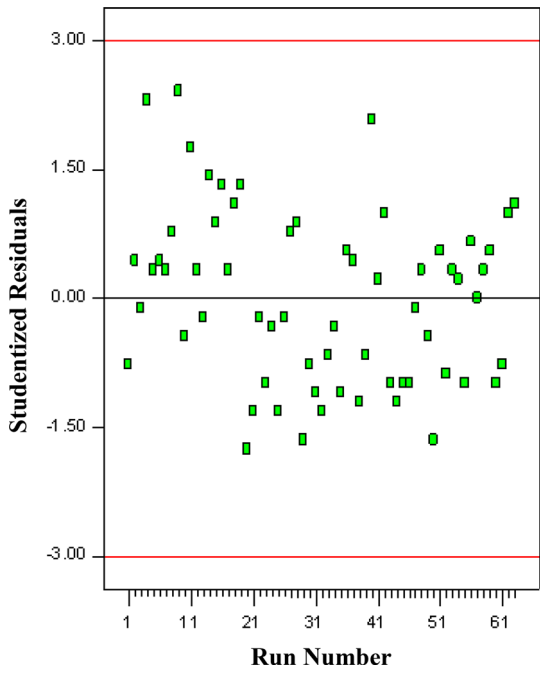


**Fig. 13** Outlier t plot of residuals for variation of MO concentration using $TiO_2$ nanoparticles

can be observed that there is no any outlier design point in the experimental data for MO concentration. Therefore, the outlier test also confirms the adequacy of the both proposed models.

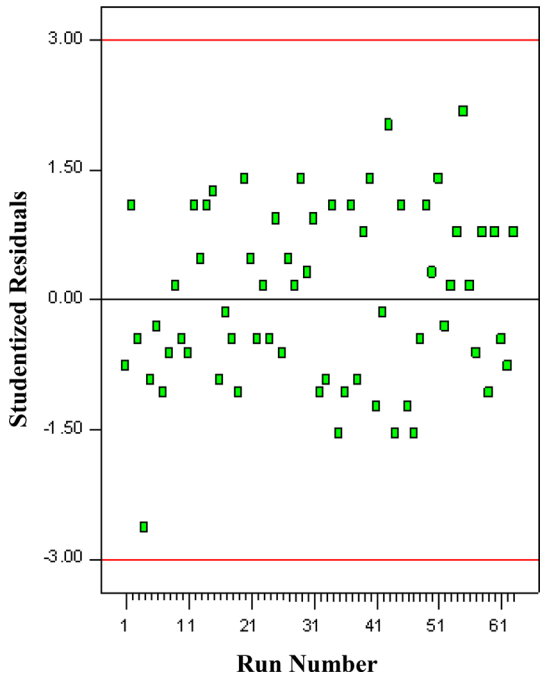


**Fig. 14** Outlier t plot of residuals for variation of MO concentration using MWCNTs@$TiO_2$

## Conclusions

The degradation rate of MO is investigated using synthesized $TiO_2$ nanoparticles and MWCNTs@$TiO_2$ as photocatalysts. The FTIR analysis confirms the vibration of Ti–O bond in the attached $TiO_2$ nanoparticles (O–Ti–O) on the surface of MWCNTs. TEM image reveals that the average particle size of the synthesized $TiO_2$ nanoparticles is in the range of from 6 to 14 nm. The influence of irradiation time and weight fraction of photocatalysts on the degradation of MO is positive. The statistical analysis results show that the effect of UV irradiation time on the decomposition of MO is higher than that of weight fraction. Meanwhile, based on the graphical analysis of the residuals, the normal distribution of residuals can be verified.

**Acknowledgements** The authors of this article express their special thanks and appreciation to the Esfarayen University of Technology.

## Compliance with Ethical Standards

**Conflict of interest** We declare that we have no financial and personal relationships with other people or organisation that can inappropriately influence our work.

## References

1. M. Ahmad, E. Ahmed, Z. L. Hong, W. Ahmed, A. Elhissi, and N. R. Khalid (2014). *Ultrason. Sonochem.* **21**, 761.

2. J. Singh, T. Dutta, K.-H. Kim, M. Rawat, P. Samddar, and P. Kumar (2018). *J. Nanobiotechnol.* **16**, 84.
3. H. Kaur, S. Kaur, S. Kumar, J. Singh, and M. Rawat (2020). *J. Clust. Sci.*
4. S. Abbasi and M. Hasanpour (2017). *J. Mater. Sci.* **28**, 1307.
5. M. Saquib and M. Muneer (2003). *Desalination* **155**, 255.
6. G. Kaur, H. Kaur, S. Kumar, V. Verma, H. S. Jhinjer, J. Singh, M. Rawat, P. P. Singh, and S. Al-Rashed (2020). *J. Inorg. Organomet. Polym. Mater.*
7. H. Kaur, V. Goyal, J. Singh, S. Kumar, and M. Rawat (2019). *Micro. Nano Lett.* **14**, 1229.
8. S. Abbasi and a. M.-S. Ekrami-Kakhki, and M. Tahari (2019). *Progr. Ind. Ecol.* **13**, 3.
9. H. Kaur, S. Kaur, J. Singh, M. Rawat, and S. Kumar (2019). *Mater. Res. Express* **6**, 095034.
10. M. Ahmad, Z. L. Hong, E. Ahmed, N. R. Khalid, A. Elhissi, and W. Ahmad (2013). *Ceram. Int.* **39**, 3007.
11. A. Ghaderi, S. Abbasi, and F. Farahbod (2015). *IJCCE* **12**, 96.
12. S. Abbasi (2016). *IJHE* **9**, 433.
13. S. Abbasi (2018). *Mater. Res. Express* **5**, 066302.
14. M. Singh, J. Singh, M. Rawat, J. Sharma, and P. P. Singh (2019). *J. Mater. Sci.* **30**, 13389.
15. S. Abbasi (2019). *J. Inorg. Organomet. Polym. Mater.*
16. K. Li, Y. Guo, F. Ma, H. Li, L. Chen, and Y. Guo (2010). *Catal. Commun.* **11**, 839.
17. S. Abbasi, F. Ahmadpoor, M. Imani, and M.-S. Ekrami-Kakhki (2019). *Int. J. Environ. Anal. Chem.* **100**, 225.
18. S. Abbasi and M. Hasanpour (2017). *J. Mater. Sci.* **28**, 11846.
19. N. Roozban, S. Abbasi, and M. Ghazizadeh (2017). *J. Mater. Sci.* **28**, 6047.
20. N. Roozban, S. Abbasi, and M. Ghazizadeh (2017). *J. Mater. Sci.* **28**, 7343.
21. S. Abbasi, S. M. Zebarjad, and S. H. N. Baghban (2013). *Engineering* **5**, 207.
22. S. Abbasi, S. M. Zebarjad, S. H. N. Baghban, and A. Youssefi (2015). *Synth. React. Inorg. M* **45**, 1539.
23. S. Abbasi, M. Hasanpour, and M. S. E. Kakhki (2017). *J. Mater. Sci.* **28**, 9900.
24. J. G. Yu, T. T. Ma, and S. W. Liu (2011). *Phys. Chem. Chem. Phys.* **13**, 3491.
25. A. Singh, V. Goyal, J. Singh, and M. Rawat (2020). *Curr. Res. Green Sustain. Chem.*.
26. S. Abbasi, M. Hasanpour, F. Ahmadpoor, M. Sillanpää, D. Dastan, and A. Achour (2019). *Int J. Environ. Anal. Chem.*.
27. S. Abbasi, S. M. Zebarjad, S. H. N. Baghban, and A. Youssefi (2014). *Bull. Mater. Sci.* **37**, 1439.
28. S. Abbasi, S. M. Zebarjad, S. H. N. Baghban, A. Youssefi, and M.-S. Ekrami-Kakhki (2016). *J. Therm. Anal. Calorim.* **123**, 81.
29. A. Ahmad, M. I. Ahmad, M. Younas, H. Khan, and M. u. H. Shah (2013). *Iran. J. Chem. Chem. Eng.* **32**, 33.
30. M. Namvar-Mahboub and M. Pakizeh (2014). *Korean J. Chem. Eng.* **31**, 327.
31. A. Ghaderi, S. Abbasi, and F. Farahbod (2018). *Mater. Res. Express* **5**, 065908.
32. J. Zhu, J. D. Kim, H. Peng, J. L. Margrave, V. N. Khabashesku, and E. V. Barrera (2003). *Nano Lett.* **3**, 1107.
33. K. Byrappa, A. S. Dayananda, C. P. Sajan, B. Basavalingu, M. B. Shayan, K. Soga, and M. Yoshimura (2008). *J. Mater. Sci.* **43**, 2348.
34. S. Abbasi (2018). *IJHE* **5**, 113.
35. S. Abbasi (2019). *Environ. Monit. Assess.* **191**, 206.
36. S. Abbasi, M.-S. Ekrami-Kakhki, and M. Tahari (2017). *J. Mater. Sci.* **28**, 15306.
37. A. H. Navidpour, M. Fakhrzad, M. Tahari, and S. Abbasi (2019). *Surf. Eng.* **35**, 216.
38. G. Zhu, H. Wang, G. Yang, L. Chen, P. Guo, and L. Zhang (2015). *RSC Adv.* **5**, 72476.
39. M. Fakhrzad, A. H. Navidpour, M. Tahari, and S. Abbasi (2019). *Mater. Res. Express* **6**, 095037.
40. M.-S. Ekrami-Kakhki, S. Abbasi, and N. Farzaneh (2018). *Anal. Bioanal. Electrochem.* **10**, 1548.
41. M.-S. Ekrami-Kakhki, S. Abbasi, and N. Farzaneh (2018). *Electron. Mater. Lett.* **14**, 70.